ELSEVIER

Chemical Physics 205 (1996) 91–108

Chemical Physics

Femtosecond time-resolved photoemission study of hot electron relaxation at the GaAs(100) surface

C.A. Schmuttenmaer [a,1], C. Cameron Miller [a], J.W. Herman [a,2], J. Cao [b], D.A. Mantell [c], Y. Gao [b], R.J.D. Miller [a,3]

[a] *Center for Photoinduced Charge Transfer, Department of Chemistry, University of Rochester, Rochester, NY 14627, USA*
[b] *Department of Physics and Astronomy, University of Rochester, Rochester, NY 14627, USA*
[c] *Xerox Webster Research Center, Webster, NY 14580, USA*

Received 17 July 1995

Abstract

Time-resolved two-photon photoemission spectroscopy is used to study the relaxation of hot electrons as a function of excitation energy for a variety of device grade and molecular beam epitaxial grown GaAs(100) surfaces. Relaxation times ranging from tens of femtoseconds to greater than 400 fs are observed depending on the energy of the intermediate state, the surface quality, and the bulk material quality. This study provides detailed information on electron relaxation dynamics in the corresponding energy range and spatial distribution along the surface normal relevant to hot electron transfer processes at interfaces.

1. Introduction

The process of excited carrier relaxation in semiconductors has been the subject of intense experimental and theoretical effort for several decades [1]. The elucidation of relaxation pathways and their associated time scales is very important from a technological standpoint as device dimensions are reduced, and begin to approach excited carrier mean free paths. In addition, carrier dynamics impose rigorous upper limits on device switching speeds. Many recent experimental studies of relaxation dynamics in semiconductors have utilized optical probes such as time-resolved luminescence spectroscopy [2–5], transient transmissivity [6–10], transient reflectivity [11], and degenerate four wave mixing [12–19]. These techniques provide femtosecond time resolution in some cases, but they do not provide direct information about the hot carrier dynamics. These methods rely on relating changes in optical properties to electron dynamics which are ill defined for highly excited electron distributions with respect to the electron energetics. In addition, techniques such as photoluminescence which can be correlated to the electron energetics generally do not have sufficient time resolution and/or sensitivity to study electron relaxation in the energy range relevant to surface field accelerated electrons, i.e., relevant to current issues regarding hot electron surface chemistry.

[1] Present address: Department of Chemistry, Yale University, New Haven, CT 06520-8107, USA.

[2] Present address: Universal Instruments Corporation, Binghamton, NY 13902-0825, USA.

[3] Present address: Department of Chemistry, University of Toronto, Toronto, Ontario M55 1A1, Canada.

SSDI 0301-0104(95)00328-2

Moreover, the various optical methods are restricted to the study of electron relaxation processes in the bulk. One might expect the surface to change the dynamics of electron relaxation significantly: the break in symmetry at the surface reduces the local density of states, the phonon distribution is perturbed, and the defect density is typically higher at surfaces. All these factors may lead to dramatically different electron relaxation dynamics in the surface region relative to bulk processes. For many solid state devices and for surface photochemistry, it is the non-radiative relaxation of electrons in the near surface region (10–100 Å from the surface) which is most relevant. This relaxation information is needed to determine the competing channels to hot electron processes and to better elucidate the operating time scales. These dynamics, in turn, determine the branching ratio between hot and thermalized electron product states. Currently, the key question is how significant is this surface effect on the electron dynamics. If the surface condition affects the dynamics, it may be possible to control to a certain degree the electron relaxation processes by modifying the surface structure. In this regard, time-resolved two-photon photoemission spectroscopy (TR-PES) is an attractive alternative to other techniques because it is capable of directly measuring the dynamics of excited carriers on an ultrafast time scale in the surface region. This technique has been used previously by several research groups to study carrier relaxation at metal and semiconductor surfaces [20–26]. Important insights have been gained in understanding surface band structure, interfacial trapping, and electron relaxation through these studies. In the present work, the emphasis is on the relaxation of highly excited electrons (> 0.5 eV excess energy) which can not readily be obtained with the above mentioned all-optical methods.

One of the primary advantages of TR-PES compared to other techniques is that it is possible to measure electron dynamics as a function of excited state energy, rather than simultaneously convoluting together the dynamics of all the excited states that are populated. The dynamical information is obtained with fewer ambiguities. Thus, both the energetics and dynamics of the excited electron distribution can be determined simultaneously, in the surface region of interest. In addition, with current laser technology, the temporal resolution can exceed 10 fs which is sufficient for full characterization of these dynamics. In this paper, we utilize TR-PES to study the dynamics of electron relaxation in GaAs(100), a direct bandgap semiconductor. GaAs(100) is an important model surface as recent in situ studies of interfacial hole transfer have observed dynamics which are competitive with electron thermalization (based on bulk dynamics) [27]. This observation supports the basic tenets of the hot electron model for fully optimized solar energy conversion strategies [28]. To determine the upper limits of the branching ratio between hot electron and thermalized electron product states, the competing electron thermalization dynamics need to be characterized at the surface and compared to adiabatic interfacial electron transfer limits. In this problem, the hot electrons are produced through field acceleration in the surface space charge field and arrive at the surface with excess energies on the order of 1 eV. The relaxation dynamics depend strongly on the electronic density of states which is energy dependent. The electron relaxation dynamics in this excess energy range have yet to be characterized at either the bulk or surface with sufficient time resolution. In addition, GaAs(100) interfaces are used extensively in solid state devices. Here again, the dynamics of hot electron relaxation at the interface are an important prelude to ballistic electron devices. In this study, both device grade and molecular beam epitaxial (MBE) grown GaAs(100) surfaces are studied to determine the dependence of the relaxation process on material properties and surface quality. These comparisons to results of those corresponding bulk studies exploiting all-optical methods provides new insight into the role the surface plays in the non-radiative relaxation of excited electronic states.

2. Experimental

The experimental system was previously utilized to measure the excited state electron lifetimes in Cu(100) and is described in more detail elsewhere [23]. The major components of the experimental apparatus consist of an ultrahigh vacuum (UHV) chamber and a femtosecond laser system. The UHV

system has a base pressure of 1×10^{-10} Torr. The cleanliness and long range order of the samples are assessed using X-ray photoelectron spectroscopy (XPS) and reflection high-energy electron diffraction (RHEED). The samples are mounted on a manipulator with five degrees of freedom that is equipped with both an electron beam heater and liquid nitrogen cooling. The sample temperature is monitored with a thermocouple mounted in proximity to the sample. Detection of the photoelectrons is accomplished with a 100 mm inner radius hemispherical energy analyzer (Haraeus EA10) with its entrance axis parallel to the surface normal. The sample is biased at -3 or -6V for these studies in order to eliminate the effects of stray fields. A transmission energy of 10 or 20 eV is used, leading to an energy resolution of approximately 0.1 or 0.2 eV, respectively. The hemispherical energy analyzer is interfaced to a personal computer via a multichannel scalar board (EG&G Ortec).

Ongoing studies of photoemission from a variety of metals, which are not affected by surface photovoltages, have determined the work function of the energy analyzer to be 4.2 eV through the relation $\Phi_A = 2h\nu - V_{bias} - KE_{max}$, where Φ_A is the work function of the analyzer, $h\nu$ is the photon energy, V_{bias} is the applied bias voltage, and KE_{max} is the maximum electron kinetic energy measured by the analyzer. The energy of the Fermi level above the valance band maximum (VBM) for a particular sample can be determined by measuring the kinetic energy at the falling (high energy) edge of the photoemission spectrum since the photon energy, the work function of the analyzer, and the bias voltage are all known.

The laser system used for the experiments consists of a self-mode-locked, unamplified Ti : sapphire laser (Spectra Physics) which is capable of producing pulses of < 50 fs. The repetition rate of the laser is 82 MHz and the energy per pulse is approximately 10 nJ. The laser is tunable from 730 to 860 nm. For the experiments described here, the fundamental wavelength was typically 770 nm. A portion of the fundamental is frequency doubled in a 250 μm thick beta barium borate (BBO) crystal (Quantum Technology) or a 600 μm thick LBO crystal (Eastek International) and is double-passed through a prism pair to compensate for group velocity dispersion [29]. The resulting beam (385 nm, 3.2 eV photon energy) is divided into two equal intensity portions with a non-polarizing beamsplitter. The two beams pass through fixed and variable optical delays, respectively, and are spatially overlapped on the surface of the sample after passing through a fused quartz viewport on the vacuum chamber. The two beams are linearly polarized and the polarization of each can be independently varied. The beams are incident at approximately a 45° angle with respect to the surface normal of the sample. The pump and probe beams are spatially overlapped at the plane of the sample surface. Time-resolved photoemission spectra for a given electron kinetic energy are obtained by varying the position of the variable optical delay line, and hence the time interval between the arrival of the excitation and probe pulses.

This study contrasts the excited carrier dynamics of samples that are MBE grown with that of those that are melt grown, hereafter referred to as device grade samples. The device grade samples are cut from n- and p-type GaAs(100) wafers with doping levels of 10^{18} and 10^{19} cm^{-3}, respectively (Crystal Specialties International). These samples were ultrasonically cleaned in solutions of trichloroethylene, acetone, and ethanol. They were then chemically etched for 60 seconds in a solution of $1 : H_2SO_4 : 8H_2O_2 : 500$ deionized H_2O, after which they were annealed in air at 475 K for approximately three minutes. The samples were then placed in the UHV chamber and further cleaned in situ with cycles of Ar^+ sputtering (3 kV for 20 minutes, 2 kV for 10 minutes, 1 kV for 10 minutes) followed by annealing (775 K for 30 minutes) until acceptable levels of cleanliness and surface order were achieved, as indicated by XPS and RHEED. The MBE-grown samples consist of a surface quantum well (QW) fabricated at the University of Rochester [30]. The samples are formed on an n-type GaAs(100) substrate, on which a 2 μm undoped GaAs(100) layer is deposited, followed by a 1 μm layer of undoped $Al_{0.4}Ga_{0.6}As(100)$, and finally a 75 or 200 Å undoped GaAs(100) layer defining the surface QW. The samples are then capped with amorphous As which is later removed by heating the samples to 675 K for 10 minutes yielding a high quality surface with orders of magnitude fewer surface states than observed for melt grown crystals.

3. Results

3.1. Kinetic energy spectrum

With the variable optical delay line set at time zero, the hemispherical analyzer scans the transmission kinetic energy providing a two photon photoemission spectrum versus electron kinetic energy. The kinetic energy spectrum for a 200 Å GaAs surface QW after accounting for the −3 V bias voltage and the 4.2 eV work function of the analyzer is shown in Fig. 1. There are two types of transitions in a two photon photoemission spectrum: direct transitions and phonon-assisted indirect transitions [31]. A continuous distribution of intermediate states in the two-photon process is accessed by direct transitions from the populated valence band states along (1/2)L − Γ to L. The 3.2 eV photons access these levels due to the nearly parallel bands in that region of momentum space. There are several other direct transitions near Γ as well as along Λ, Δ, and Σ [32]. Phonon assisted indirect transitions have the effect of randomizing the momentum distributions. Coupled with the fact that the applied bias voltage results in angle-integrated photoemission, as well as the 0.1 to 0.2 eV energy resolution of the electron analyzer, the measured two photon photoemission spectrum consists of a single feature roughly 1.4 eV wide. For the purposes of these experiments, these excitation conditions initially prepare an excited electron distribution with excess energies relevant to the surface photochemistry.

It should be noted that the photoemission spectrum shifts to lower energy, without changing in width or shape, as a function of illumination intensity by a secondary laser beam. More importantly, the secondary illumination *does not* alter the electron relaxation dynamics. This paper is primarily concerned with the electron dynamics in GaAs, so only a brief description of the photovoltage shifts will be given here. The full details of these effects are given elsewhere [33].

The photoelectron kinetic energy data are collected relative to the Fermi level, and band bending

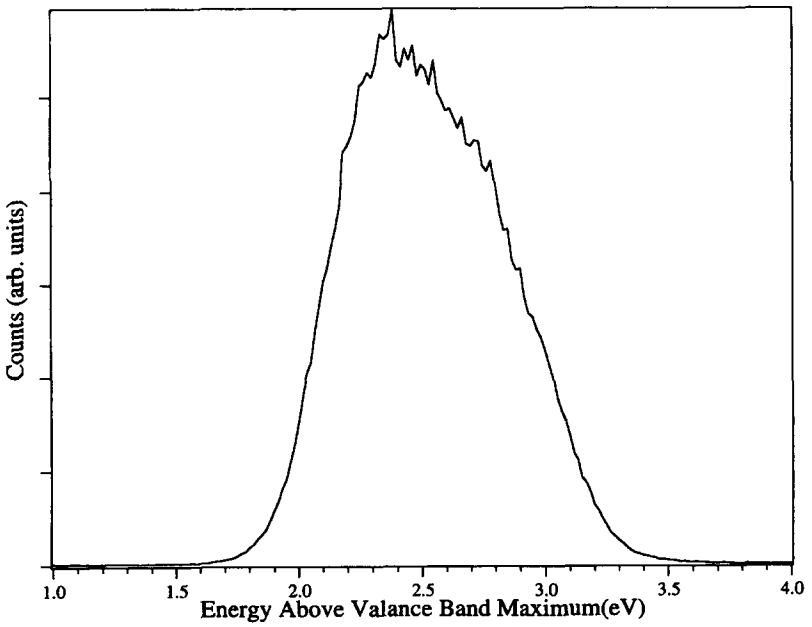

Fig. 1. Room temperature two photon photoemission spectrum for a 200 Å GaAs surface QW obtained with a photon energy of 3.2 eV (385 nm).

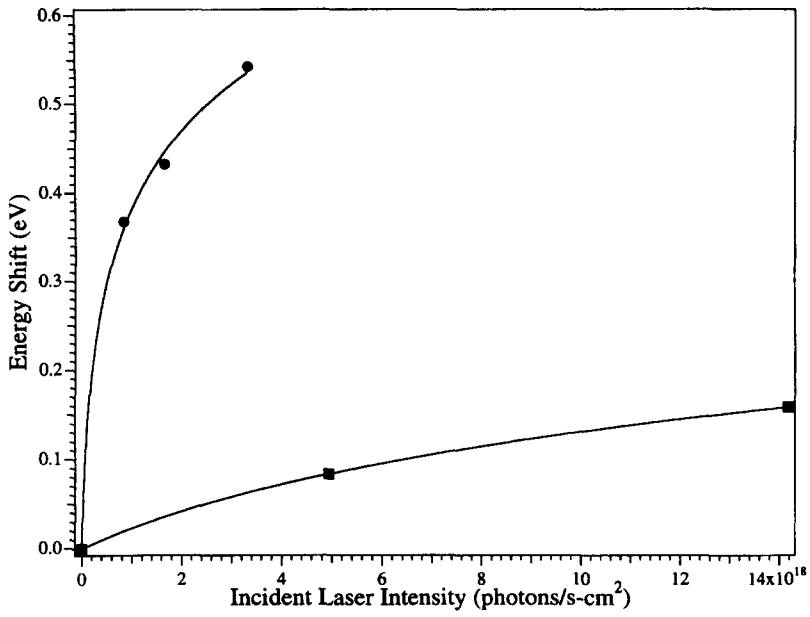

Fig. 2. Energy shifts of the spectra versus the number of photons/s cm^2. The circles show the shifts measured when using the HeNe laser, and the line through them is the result of optimizing Eq. (2). The squares show the shifts measured when varying the total intensity of the pump and probe beams, and the line through them is the result of optimizing Eq. (3).

will manifest itself as a shift in the position of the photoemission spectrum. The energy scale of the photoemission spectrum plotted in Fig. 1 is relative to the VBM, with the concomitant result that overall energy shifts are not evident. This shift is not due to the usual surface charging effects encountered when studying photoemission from insulators because in this case it is induced by photons that are above band gap, yet below the photon energy required for photoemission. This shift is not dependent on the synchronization of the pulses of the secondary illumination laser with the pump and probe pulses. In fact, a cw helium–neon (HeNe) laser also causes this effect. Fig. 2 displays this shift as a function of number of photons/s cm^2 for illumination with a HeNe laser as well as simply increasing the total power in the pump and probe beams.

A photocurrent-dependent photovoltage shift has been previously measured for GaAs [34]. In that work, the magnitude of the shift (ΔV) is quantitatively described by

$$\Delta V = E_0 \ln\left(\frac{J(I)}{J_0}\right), \tag{1}$$

where E_0 is dependent on the dominant current flow mechanism of the material, J_0 is the restoring current of the experiment, and $J(I)$ is the photocurrent density which is proportional to the number of carriers. In the case of HeNe illumination, the restoring current, J_0, is proportional to the number of carriers, N_0, intrinsic to the material and that from the pump and probe beams. The photocurrent density, $J(I)$, is proportional to $N_0 + N_{\mathrm{HeNe}}$, where N_{HeNe} is the additional number of carriers due to the incident HeNe illumination. The number of carriers generated by the HeNe laser is proportional to the intensity of the HeNe laser. Eq. (1) can then be expressed as

$$\Delta V = E_0 \ln\left(\frac{N_{\mathrm{HeNe}}}{N_0} + 1\right). \tag{2}$$

Similarly, if the excess carriers are generated by increasing the total intensity of the pump and probe beams, rather than using a secondary laser, the photovoltage shift will be given by

$$\Delta V = E_0 \ln\left(\frac{N_{\mathrm{P-P}}}{N_0} + 1\right). \tag{3}$$

In this case, N_0 is the number of carriers intrinsic to the material and that from the least intense pump and probe beams used to make the measurement, and N_{P_P} is the additional number of carriers due the increase in pump and probe intensity above the minimum intensity required to make the measurement. Data for both of these cases are plotted in Fig. 2, along with the results of a nonlinear least squares fit of Eqs. (2) and (3). The quantities E_0 and N_0 were iteratively varied in the nonlinear least squares fits to produce the solid lines shown in Fig. 2. For the optimization of Eq. (2), E_0 was determined to be 0.132 ± 0.015 eV and N_0 was determined to be $5.2 \times 10^{16} \pm 2.1 \times 10^{16}$ photons/s cm^2. Optimization of Eq. (3) leads to $E_0 = 0.1062 \pm 0.0004$ eV and $N_0 = 4.110 \times 10^{18} \pm 0.026 \times 10^{18}$ photons/s cm^2.

The most important conclusion regarding the photovoltage shift is that the electron dynamics are *not* affected. Fig. 3 presents the electron relaxation dynamics for two extreme levels of secondary illumination with a HeNe laser. Even though the raw photoemission spectrum had shifted by 0.5 V due to the intensity of the HeNe laser beam, the electron relaxation dynamics are identical.

Fig. 4 illustrates typical data taken for device grade samples. The data presented is from n-type GaAs(100) with a doping level of 10^{18} cm^{-3}, and p-type with doping of 10^{19} cm^{-3}. These spectra have a much more pronounced high energy tail than the surface QWs due to lower surface quality. The lower surface quality creates mid-gap states very close to the valance band maximum. The populated mid-gap states are excited in the two photon photoemission producing a high energy tail. To verify the doping conditions in the surface region, these samples were studied as a function of temperature. The spectrum shifts as the sample is heated from 120 to 510 K in a manner consistent with the temperature dependence of the Fermi level for n- and p-doped materials. The temperature-dependent energy shift in the photoemission spectra is due to the well known dependence of the Fermi level on temperature, and is determined by the type of dopant and its concentration [35]. For n-type semiconductors at high temperatures the Fermi level decreases and approaches the intrinsic mid-gap level, while for p-type semiconductors the Fermi level increases and approaches mid-gap at high temperatures. We measured a shift of 0.56 eV for the n-type material, and a 0.41 eV shift for

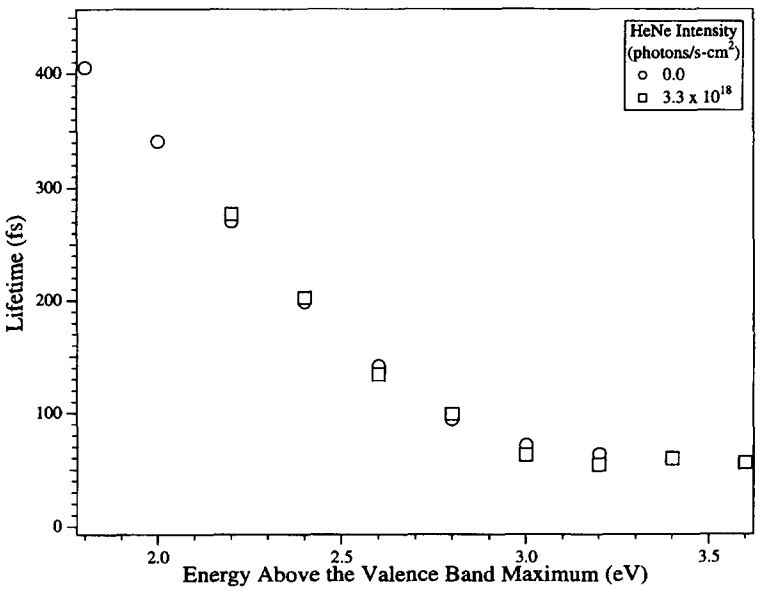

Fig. 3. The electron lifetimes for a 200 Å surface QW versus kinetic energy with and without HeNe laser illumination. The circles represent the lifetimes without HeNe illumination, and the squares are the lifetimes with 3.3×10^{18} photons/s cm^2 of HeNe illumination.

the p-type material in changing the temperature from 120 to 510 K. This study was conducted as an additional control as there were only minor differences observed in the electron relaxation dynamics for these two materials despite the differences in field polarity of the space charge field at these two surfaces. For n-type material, the space charge field due to surface state charging would lead to field assisted transport of electrons away from the surface and thus lead to a faster *apparent* relaxation of the excited electron distribution. In contrast, the p-type surface should block transport away from the surface. Assuming a dark state space charge field of 1 eV (10^{12}–10^{13} charges/cm^3), the photoexcitation conditions are expected to cause significant screening at these single crystal surfaces. The photoemitted spectrum from the device grade samples did not shift under the excitation conditions studied, and the dynamics were comparable for the n- and p-type materials which is consistent with this expectation. The results for the device grade surfaces are in contrast to the MBE grown materials in which more electron accumulation can occur in the surface quantum well, or epilayer, than in the surface states of the single crystals [36].

3.2. Pump–probe spectra

Pump–probe scans are taken at various electron kinetic energies throughout the two photon photoemission spectrum. These data are obtained by fixing the energy window of the hemispherical energy analyzer at a given value and recording the number of photoemitted electrons as a function of delay time between the excitation and probe pulses. The electron kinetic energies are referenced to the location of the VBM. A photoexcited carrier density of 1×10^{18} cm^{-3} is estimated for 10 mW power of 385 nm light on the GaAs sample, with a beam diameter of 150 μm and an optical skin depth of 135 Å [37]. The energy of the measured intermediate state above the VBM, $E_i - E_{VBM}$, is determined from the falling (high energy) edge of the spectrum and the photon energy. The falling edge of the two photon photoe-

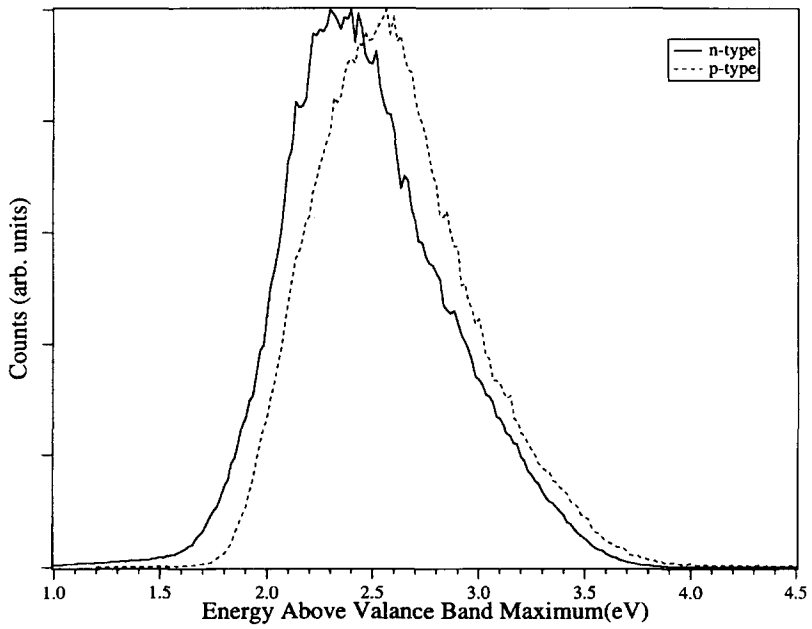

Fig. 4. Room temperature two photon photoemission spectrum for n-type GaAs(100) (solid line) with a doping of 10^{18} cm^{-3} and p-type GaAs(100) (dashed line) with a doping of 10^{19} cm^{-3}.

mission spectrum occurs when the intermediate state is at one photon energy above the VBM. The instrument response function is determined by performing a pump–probe scan using a Pt surface while monitoring a high electron kinetic energy (3.0 eV above the fermi level), where the electron relaxation dynamics are extremely fast. Typically, the temporal width of the instrument response function scan is comparable to the full-width at half-maximum (FWHM) of the autocorrelation of the fundamental (770 nm) laser pulse. The fact that our system is instrument response limited for a metal surface at higher electron kinetic energies was previously demonstrated on Cu(100) [23]. The instrument response function, which varies with the pulsewidth of the laser, is obtained for each set of data.

Fig. 5 presents three representative pump–probe scans taken at room temperature using the 200 Å GaAs surface QW. The three pairs of scans in Fig. 5 correspond to the highest energy accessible, an intermediate energy, and the lowest energy accessible (3.2, 2.6, and 2.0 eV above the VBM, or equivalently 1.8, 1.2, and 0.6 eV of excess energy above the CBM, respectively). At each energy, one scan with the pump and probe lasers polarized parallel to each other, and one with the pump and probe beams polarized perpendicular to each other is shown. There is a pronounced variation in the electron relaxation dynamics at the three energies shown. The relaxation occurs on a 50 to 60 fs timescale at high energy, on a 100 fs timescale at intermediate energies, and on a 400 fs timescale at the lowest energies. Furthermore, there is a striking difference between the parallel polarized pump–probe data and the crossed polarized data at low energies. A sharp, laser pulsewidth limited feature exists at $\Delta t = 0$ when the beams are parallel polarized which is barely discernible when they are crossed polarized. This pulsewidth limited feature corresponds to the coherent artifact often observed in four wave mixing, pump–probe, or other time resolved experiments. This signal is related to electronic polarization induced in the material by the two excitation fields that lead to the photoemission signal. This signal decays due to electronic dephasing. Since the excitation pulse prepares a wide distribution of excited electronic states that utilize the entire spectral width of the pulse at $\Delta t = 0$, the electronic dephasing is equivalent to the pulse auto-

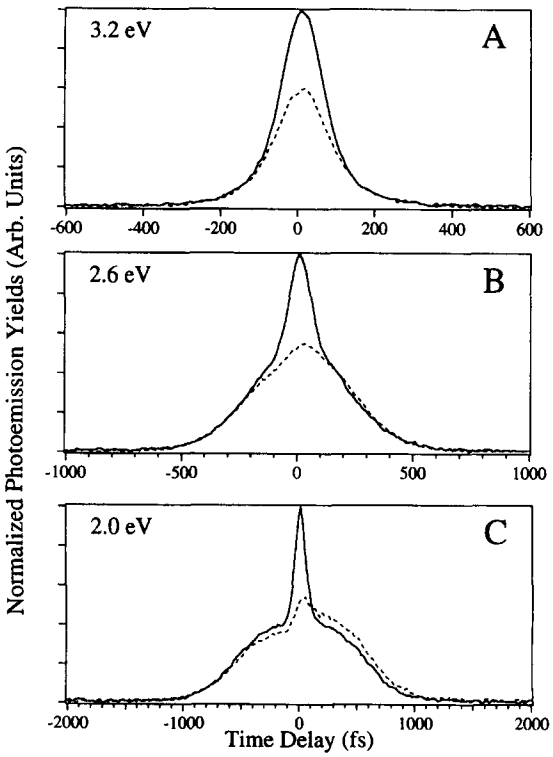

Fig. 5. Typical pump–probe scans for the surface QWs at room temperature. The energy of the intermediate state above the VBM is 3.2, 2.6, and 2.0 eV, in panels A, B, and C, respectively. Each panel has two lines: The solid line corresponds to the pump and probe lasers polarized parallel to each other, and the dashed line corresponds to them having orthogonal polarizations. The orthogonal polarized scans are slightly asymmetric due to the absorption coefficients of the surface for s and p polarized light.

correlation. Usually this feature obscures the fast dynamics of interest; however as can be seen from Fig. 5 the use of crossed polarized excitation and probe beams eliminates this complication. The effectiveness of the crossed polarization protocol is most clearly observable at the lowest excited electron energies where there is a clear separation in time scale between the coherent electronic polarization and the signal due to the excited electron population. The excited state lifetimes are reported after comparing the parallel and crossed polarizations pump–probe scans and removal of the coherent contribution to the signal.

With the above procedure the dynamics of the excited state electron distribution can be determined as a function of energy. The dynamics at high intermediate state energy are very well described by an

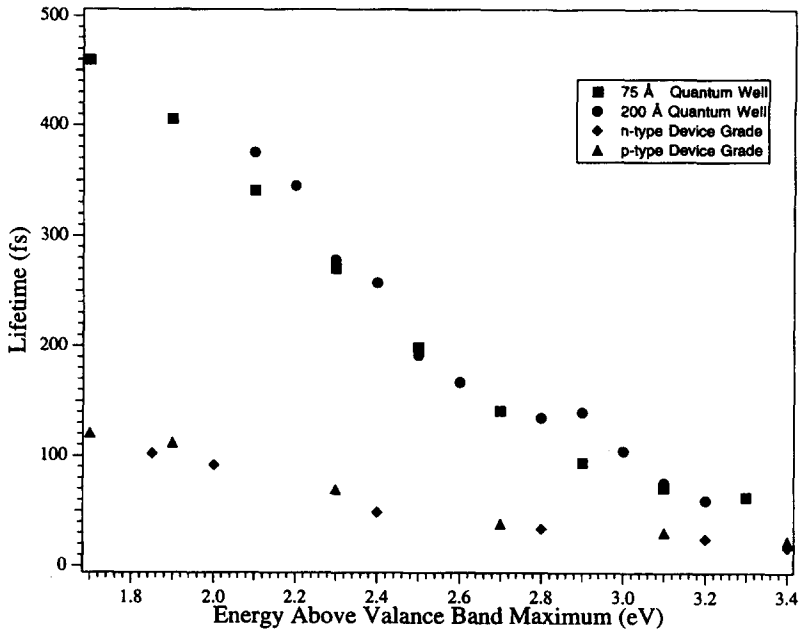

Fig. 6. The lifetime measurements of the 75 Å surface QW (squares), 200 Å surface QW (circles), n-type device grade (diamonds) and p-type device grade (triangles) are presented. The pump and probe beams are orthogonally polarized in order to avoid a contribution from the coherent artifact. Notice that the device grade samples have significantly shorter lifetimes than the surface QWs.

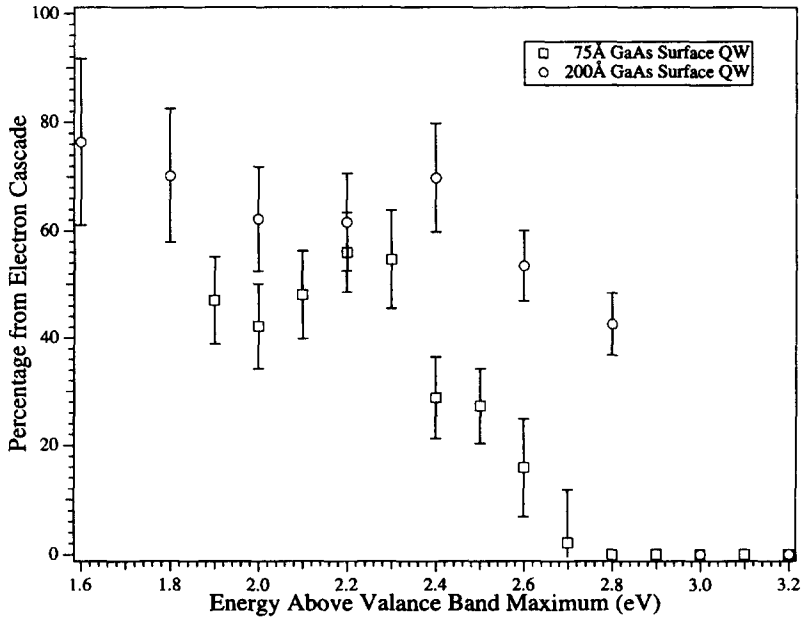

Fig. 7. The plot shows the fitting parameter P_1 divided by $P_1 + P_2$ with respect to energy above the VBM for the 200 Å (circles) and 75 Å (squares) GaAs surface QWs.

exponential decay convoluted with the Gaussian autocorrelation function, but the dynamics at low energy can not be described in this way. Along with the coherent artifact, a broad pedestal is present that is not exponential in shape but has a more Gaussian character. The evolution of the dynamics from single exponential to Gaussian can be explained as follows: the initial excitation pulse populates a continuous distribution of excited intermediate states which can then relax into the lower energy intermediate states in the continuous distribution. Therefore, in addition to relaxation mechanisms out of the lower energy intermediate states, there are also repopulation mechanisms from the states that lie above. The dynamics of these states can be adequately modeled by a simple expression with one rate constant describing the population flowing into a state and another one out of it, in the scheme $A \rightarrow B \rightarrow C$, where state B is being monitored. The population of state B is [38]

$$B = A_0\left(\frac{\tau_2}{\tau_1 - \tau_2}\right)\left[\exp\left(-\frac{t}{\tau_1}\right) - \exp\left(-\frac{t}{\tau_2}\right)\right] + B_0 \exp\left(-\frac{t}{\tau_2}\right), \tag{4}$$

where A_0 is the population that is originally placed in state A, and B_0 is the initial population of state B. The population in state C is irrelevant because once it decays into C it can never return to B (low excitation limit). The factors τ_1 and τ_2 refer to the exponential time constants of electron relaxation into and out of the intermediate state B, respectively. The continuous distribution of initially populated states relax into the lower energy states, which requires that Eq. 4 be integrated over the distribution of high energy states that lie above the state in question. The distribution $A_0(E)$ which is the initial population distribution is equal to the kinetic energy spectrum taken at $\Delta t = 0$. The lifetime of the highest energy state is modeled by a simple exponential decay because there are not any states lying above this level that could repopulate it. For the next highest level, the lifetime measured for the highest level becomes τ_1, and τ_2 is determined for that level. For subsequent levels, τ_1 is a distribution with respect to excess energy, and determining τ_2 requires the following integration. The population of state B is

$$B = P_1\left\{N_1 \int_{E_B}^{E_{\max}} \frac{A_0(E)\tau_2}{(\tau_1(E) - \tau_2)}\left[\exp\left(-\frac{t}{\tau_1(E)}\right) - \exp\left(-\frac{t}{\tau_2}\right)\right] \mathrm{d}E\right\} + P_2\left[N_2 B_0 \exp\left(-\frac{t}{\tau_2}\right)\right], \tag{5}$$

where $E_{\max}$ is the maximum energy of the distribution populated by the excitation pulse, E_B is the energy of state B, and N_1 and N_2 are normalization constants. P_1 and P_2, the fitting parameters, and τ_2, the lifetime of state B, are optimized in a nonlinear least squares fit to the data. When the experimental data is modeled, Eq. (5) is also convoluted with the Gaussian autocorrelation function. To determine the lifetimes for a set of data, the optimization proceeds from highest to lowest energy because the distribution $\tau_1(E)$ that describes the population flowing into a level needs to be constructed from the higher energy levels. An assumption of this analysis is that a higher energy state relaxes to any lower state weighted by the initial population distribution. The data do not currently warrant a more complex scheme of statistical weighting considering the relatively small energy differences involved. The distribution of $\tau_2(E)$ represents the lifetimes of the levels as a function of energy above the VBM. The lifetimes determined for the 200 and 75 Å GaAs surface QWs are shown in Fig. 6. The contribution to the pump and probe scan from the cascading electrons as a function of energy above the VBM is represented by the ratio $P_1/(P_1 + P_2)$, and is plotted in Fig. 7. At lower energies, the contribution from higher energy electrons cascading into the lower energy electron populations is greater than 50%.

Fig. 8 displays representative room temperature pump–probe scans of the device grade GaAs(100) samples analogous to Fig. 5. Again, the scans shown are taken at high, intermediate, and low kinetic energies, with both parallel pump–probe and crossed pump–probe arrangements shown. There are several notable differences between these scans and those

for the surface QWs. First, the range of time scales for the dynamics is much smaller. The high energy scans have relaxation on the 20 fs timescale, and the low energy scans are on the 100 fs timescale. Second, the development of a pedestal with a coherent artifact at low energy does not occur because the relaxation time is too short. Next, the excited electronic state lifetimes in the n-type sample at two sample temperatures ($T = 120$ K and $T = 510$ K), and for both parallel and orthogonal polarized excitation and probe beams were measured. The lifetimes obtained with orthogonal pump and probe beams do not show significant dependence on the temperature of the sample due to the already rapid relaxation. We also measured the excited electron lifetimes for the p-type sample at room temperature with both parallel and crossed excitation and probe beams and similar

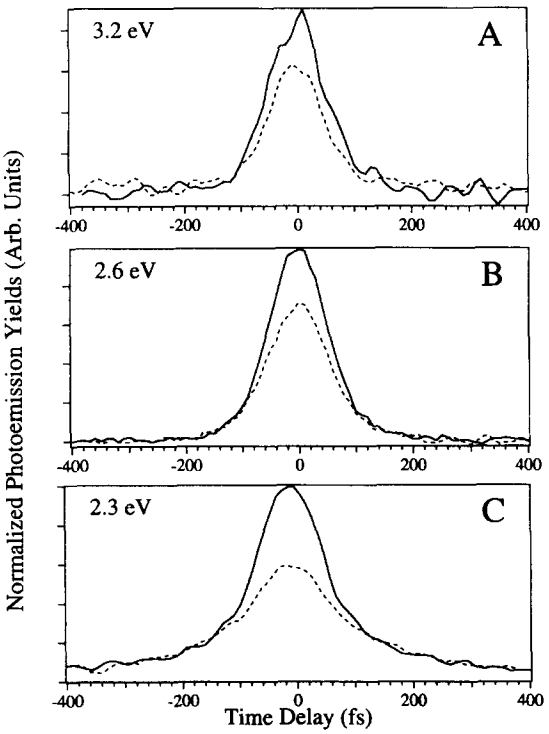

Fig. 8. Typical pump–probe scans for device grade GaAs(100) at room temperature. Data for the n-type doping are displayed, and the dynamics for the samples with p-type doping are similar. The energy of the intermediate state above the VBM is 3.2, 2.6, and 2.3 eV, in panels A, B, and C, respectively. Each panel has two lines: The solid line corresponds to the pump and probe lasers polarized parallel to each other, and the dashed line corresponds to them having orthogonal polarizations.

results were obtained. All the data taken with device grade material were modeled with a single exponential decay, since the relaxation is so rapid. There are features to the signal reminiscent of a relaxation process cascading from higher energy levels to lower energies, but are not strong enough to warrant a numerical fit. The exponential decay time constant for the device grade samples, as well as $\tau_2(E)$ for the surface QWs is displayed in Fig. 6. The origin of the differences between the surface QW data and that for the device grade samples is discussed in Section 4.

3.3. Thermalization rate

The initial excitation pulse populates a non-equilibrium distribution of states. As time progresses, the distribution approaches a Fermi–Dirac distribution. The amount of time the system takes to thermalize is directly affected by the relaxation mechanisms. Very similar studies have been conducted at the Si(100) surface by Goldman and Prybyla [22]. For Si, a non-thermal component to the measured distribution was not distinguishable at a delay of 120 fs [22], which indicates that the electron–electron scattering time must be less than 120 fs. For GaAs, luminescence studies have shown that electrons in the Γ valley equilibrate within 100 fs [2]. The main mechanism of thermalization was attributed to inelastic electron–electron scattering because of the absence of any spectral features in the luminescence with spacing equal to the optical phonon energy [2]. In the present study, the population distribution for specific delays is determined from the orthogonally polarized pump–probe data by normalizing it to the kinetic energy spectrum and examining the photoemission yield at specific temporal delays. Fig. 9 displays the population distributions as a function of energy above the conduction band minimum (CBM) for several different pump–probe delay times. Fig. 9 also presents calculated population distributions obtained for a density of states that is proportional to the square root of energy above the CBM that follow a Fermi–Dirac distribution:

$$N_i \propto (E_i - E_{\mathrm{CBM}})^{1/2} \times \left(\frac{1}{1 + \exp[(E_i - E_{\mathrm{CBM}})/kT]} \right), \qquad (6)$$

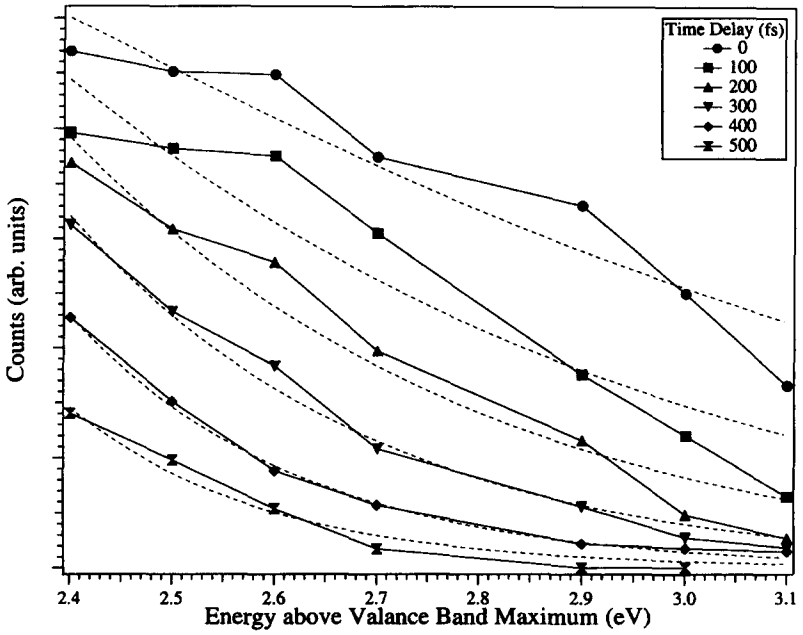

Fig. 9. Population distributions in the surface QW sample as a function of energy above the CBM. The circles correspond to a delay of 0 fs, the squares correspond to a delay of 100 fs, and the delay increases by 100 fs for each subsequent symbol. The dashed lines are Fermi–Dirac distributions as given by Eq. (6), optimized to the data by varying the normalization constant and electron temperature.

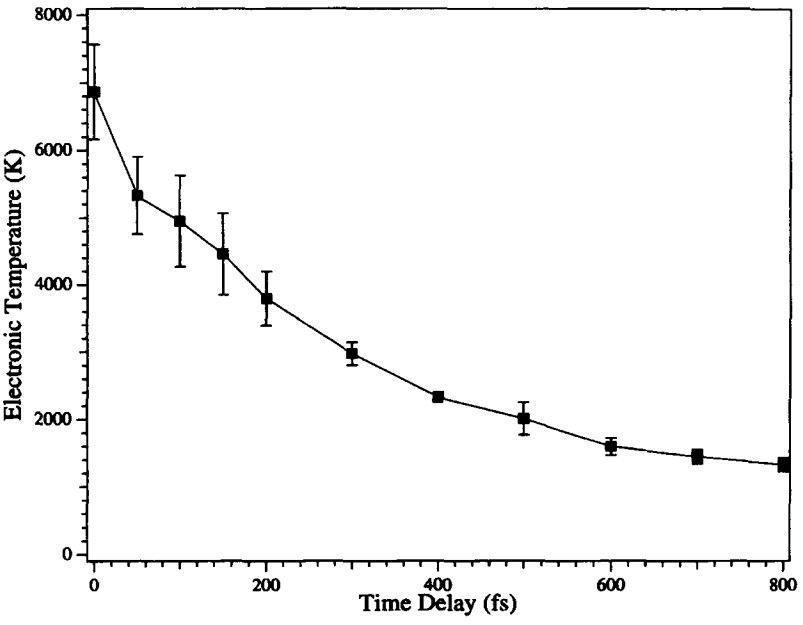

Fig. 10. The electron temperature as a function of the pump–probe delay. Note that the error bars are large at early time, indicating a non-equilibrium distribution that is not adequately modeled by a Fermi–Dirac thermal distribution.

where N_i is the population at energy E_i, E_{CBM} is the energy of the CBM, k is Boltzmann's constant, and T is temperature. Thus, the normalization constant and temperature are obtained through a nonlinear least squares fit. By 300 fs, the photoexcited electron population has largely thermalized, based on the agreement of the experimental data with the functional form shown in Eq. (6), as seen in Fig. 9.

The contribution of the electron–electron scattering can be determined by examining the temperature of the free electron gas. Fig. 10 shows the temperature of the free electron gas as a function of time obtained by fitting Eq. (6) to the experimental data. The distribution thermalizes in about 300 fs, largely due to the electron–electron scattering [39]. After that time, energy is dissipated to the lattice as heat through electron–phonon scattering. The temperature is not well defined prior to 300 fs since the electrons have not yet achieved a thermal distribution, and this is reflected in the large error bars at early times in Fig. 10.

4. Discussion

The surface QW samples are discussed first because there is a wider range of dynamics as a function of electron energy with these samples compared to that for device grade materials. This system then provides a basis for interpreting the electron dynamics observed for the device grade samples.

The dynamics for the 200 Å sample and 75 Å sample are identical. This initially surprising result provides several important pieces of information. First, it confirms that the escape depth of photoelectrons is roughly 50 Å. Since any photoemission measurements require that an electron escape from the sample, these measurements are not directly sensitive to features that exist further from the surface than the escape depth. Second, the low spectral resolution of the experiment, due to the bias voltage, analyzer pass energy, and the short laser pulsewidth, preclude observation of quantum effects that are often seen in the luminescence spectra of QW samples. Finally, and most importantly, the quantization is only in one dimension (along the surface normal) which leaves a large and continuous distribution of states in the other two dimensions, and these unquantized states dominate the relaxation dynamics. Thus, changing the thickness of the surface QW should not, and does not, significantly affect the measured dynamics. This effect has been observed previously in comparing bulk GaAs to superlattice and multiple GaAs QW structures [3,4]. The only differences occur at higher injection levels than used in this study in which case a hot phonon bottleneck slows the electron cooling dynamics [3,4].

One of the most striking features of the measurements using the surface QWs is the coherent artifact in the pump–probe scans taken at low electron kinetic energy (see Fig. 5). This feature is clearly resolved in the other low kinetic energy scans that were not included in the figure, and the width is constant at all of these energies. The electronic dephasing time for the initially prepared excited electron distribution must therefore be equal to or shorter than 20 fs. As the electron relaxation dynamics become faster at higher electron energy, it becomes impossible to separate this electronic dephasing process from the relaxation. The assertion that this spike is due to electron dephasing is supported by the fact that it is only observed when the pump and probe pulses are polarized parallel to each other, while the signal at longer times, which is ascribed to relaxation dynamics, is present regardless of whether the pump and probe pulses are polarized parallel or perpendicular to each other. Furthermore, four wave mixing studies find the polarization dephasing time to be 20 fs for a carrier density of 1×10^{18} cm^{-3}, which is consistent with these observations. The rapid electronic dephasing is also expected based on the broad distribution of electronic states prepared by the 3.2 eV excitation pulse as evident in the photoemission spectrum.

The high surface quality results in long excited electron lifetimes. In the presence of surface traps, the excited state lifetime is greatly reduced, as seen with the device grade samples. The work function (and consequently, the electron affinity), is strongly dependent on the surface quality, and can therefore be used as another diagnostic. The measured electron affinity of the MBE-grown surface QWs is 4.0 eV which is in good agreement with previous studies and also indicates that the surface is clean and free of defects.

At very short delay times, we observe a broad

photoemission spectrum (see Fig. 1). Distinct spectral features are absent even at time zero. This behavior has been observed previously in time-resolved photoluminescence studies of GaAs with 100 fs resolution by Elsaesser and co-workers [2]. In that experiment the pump beam photon energy was 1.9 eV, exciting electrons from the split-off and heavy-hole bands to 0.2 and 0.5 eV above the CBM, respectively. The existence of broad structureless luminescence spectra led them to conclude that that the electrons in the Γ valley equilibrate within 100 fs. They concluded that inelastic carrier–carrier scattering is the dominant mechanism of thermalization in their experiment. In contrast, the 3.2 eV pump photon energy used in the present work leads to the occupation of intermediate states with energies up to 1.8 eV above the CBM. This opens up other relaxation mechanisms such as intervalley scattering.

Becker and coworkers performed a transient transmittance study of intervalley scattering rates for GaAs subjected to 2 eV excitation pulses [6]. In that study, average scattering time constants from the Γ valley to the adjacent X and L valleys of 55 and 80 fs, respectively, were obtained. A recent Monte Carlo simulation treated the femtosecond dynamics of excited carrier relaxation in bulk GaAs [40]. For high-energy (1.92 eV) excitation, they concluded that intervalley scattering is the primary carrier relaxation mechanism for the initial 50 fs, dominating other relaxation mechanisms such as carrier–carrier scattering and optical-phonon scattering [40]. Our results are consistent with a very fast intervalley scattering rate, coupled with a slower electron–electron scattering rate. Dynamics as a function of electron energy are indeed obtained here, but our experiment is not highly dependent on the momentum of the photoexcited electrons because the bias voltage on the sample integrates the photoemission over a large region of momentum space.

The range of the electron dynamics seen in the device grade samples is much smaller than that for the surface QWs. This is due to defects in the bulk and on the surface which provide many relaxation pathways. The relaxation time constants are about 5 times smaller at low energy for the device grade samples relative to the surface QWs. Further evidence that the bulk and surface material quality rather than field acceleration dominate the electron

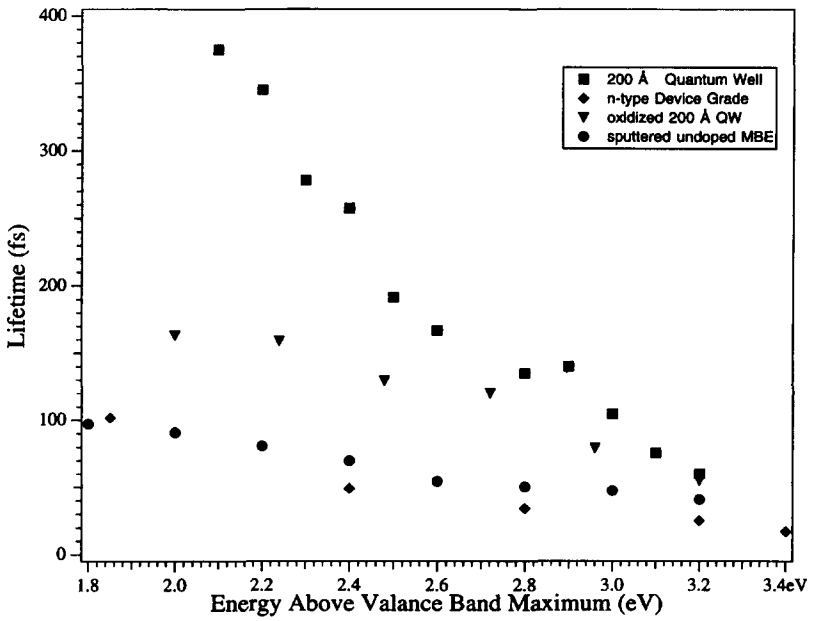

Fig. 11. The lifetime measurements of the 200 Å surface QW (squares), n-type device grade (diamonds), oxidized 200 Å QW (inverted triangles) and sputtered undoped MBE grown bulk (circles) is presented. The pump and probe beams are orthogonally polarized in order to avoid a contribution from the coherent artifact.

dynamics in the device grade samples is given by the fact that the n- and p-type samples exhibit the same behavior, as seen in Fig. 6.

The large difference in electron relaxation rates between the surface QW and bulk samples, which is almost a factor of 5 at low energy, can not be accounted for solely on the basis of quantization reducing the density of states. The quantization effect along the surface normal would only decrease the electronic density of states by 30% and this condition only applies to electron energies below the AlGaAs barrier. Furthermore, we find that the difference in quantization of a 75 and 200 Å surface QW has minimal impact on relaxation rates.

There are three differences between the two different sets of samples which should be considered as possible explanations for the dramatically different dynamics. First, the background doping in the samples is significantly different. The MBE grown samples are nominally undoped relative to high doping levels of 10^{18} cm^{-3} for the device grade samples. The initial relaxation phase is dominated by electron–electron scattering rates which obviously depends on carrier density. To check for this effect, an intensity dependent study was conducted, and to a first approximation the dynamics were invariant over the range from 10^{17} carriers/cm^3 to 10^{18} carriers/cm^3. In addition, the photocarrier injection levels for the data shown in Fig. 6 are comparable to the background doping levels of the device grade samples. Thus, the carrier density of the surface QW materials and the n-type device grade materials are in fact comparable immediately after photoexcitation. To further clarify that the doping level is not the cause of the difference in observed dynamics, a bulk MBE-grown sample was obtained and the dynamics were measured. The MBE-grown sample was prepared in the UHV chamber in a similar manner as the device grade material. Fig. 11 shows that the bulk undoped MBE grown sample has comparable dynamics to the doped device grade materials.

A second possible explanation for the different dynamics is that diffusive transport away from the surface limits the measured lifetime of the excited electron distribution for the single crystal device grade samples. The surface QW materials were specifically designed to block transport for electrons energies up to 0.3 eV above the CBM, i.e. below the AlGaAs barrier. In the higher energy range reported here, the excited electron distribution is just as free to undergo diffusive transport to the bulk as in the case of the device grade materials. There are differences in the carrier mobility in AlGaAs which may retard the diffusive transport such that this effect cannot be entirely ruled out. On the other hand, the fact that the 75 and 200 Å surface QWs yield identical dynamics strongly indicates that the differences between the device grade and surface QW samples are not due to diffusive transport.

The third possibility is that the surface is playing a role in mediating the electron transport and relaxation. To test for this contribution, a freshly decapped MBE grown GaAs(100) surface QW was allowed to oxidize. XPS spectra showed the onset of oxide growth on the surface. The oxide layer leads to a significant increase in surface states [41,42]. Prior to this exposure, the surface exhibited relaxation dynamics similar to those shown in Fig. 6. In contrast, the oxide induced surface states significantly accelerated the electron relaxation dynamics to within a factor of 2 of those observed for the device grade surfaces. These results are shown in Fig. 11. This indicates that a substantial fraction of the observed differences in dynamics is due to the surface quality and defect densities. To explain the increase in electron relaxation, the oxide-induced surface states must increase the density of electronic states involved in the scattering process. The increase in surface state densities is most readily observed in the mid-gap region of the semiconductor band structure, but these states will also affect the density of electronic states above the CBM, and this effect appears to modify the electron relaxation dynamics.

A very important observation is that electron relaxation in GaAs is as fast as in metals. This fact is interesting since the electron densities differ by over four orders of magnitude. Previously, it was noted by Fann et al. that electron dynamics in polycrystalline gold and a modulation doped quantum well were very similar. They justified their finding by emphasizing the similarity in electron screening in the two systems, as described by the quantity r_s, where small values of r_s imply a large amount of screening [20]. Alternatively, r_s describes the validity of the random phase approximation in Fermi-liquid theory [20,43], where values that are less than 1 imply that the

random phase approximation is valid. A significant result of Fermi-liquid theory is that the relaxation rate varies quadratically with excitation energy [20,43,44]. The value of r_s (in units of a_0) can be calculated using [20,43]

$$r_s = \left[\frac{3}{4\pi n}\right]^{1/3} \frac{m_e^* e^2}{4\pi\varepsilon h^2}, \quad (7)$$

where n is the total free electron density, m_e^* is the effective mass of the electron, and ε is the dielectric constant. For Au, Fann et al. found $r_s \approx 0.54$ Bohr radii [20]. For GaAs, where $n = 1 \times 10^{18}$ cm^{-3}, $m_0 = 0.067\ m_e$, and $\varepsilon = 12$, r_s is approximately 1.75 Bohr radii. These two values are very similar in magnitude compared to the factor of 10^4 difference in carrier density. Therefore, these systems have similar screening and similar relaxations even though the electron densities are four orders of magnitude different. Additional contributions to the relaxation dynamics due to the surface preparation as well as assumptions inherent in Fermi-liquid theory discourage comparisons that are more quantitative than that given above.

Inspection of the two sets of results for the surface QW and device grade surfaces shows that the relaxation rate of the surface QW samples follows a more distinct quadratic dependence on energy than the device grade samples. If one uses the CBM as the reference for defining the excess energy condition for the electrons, the observed relaxation time constants at different energies are very comparable to those observed for thin 150 Å single crystals of gold [45]. This quadratic dependence with the Fermi liquid model holds only for isotropic band structures (spherical Fermi surface). Gold is a better approximation to this than is GaAs, and specific details of the band structure and density of states should be observable in the energy dependence of the relaxation rates. This point has recently been made in the context of electron relaxation at single crystal Cu(100) surfaces [23]. Angle resolved photoemission with high resolution will be needed to see these details in GaAs.

The most important point to make in comparing the GaAs surface QW to the melt grown device grade material is that a surface effect accounts for the difference in relaxation rates. With this additional scattering process taken into account, the observed dynamics within the first few hundred femtoseconds is understandable based on electron–electron scattering, i.e., Fermi-liquid theory. Extremely rapid electron–phonon scattering processes as invoked for similar studies of electron dynamics at the Si(100) surface [22], are not needed to explain the present results.

5. Conclusion

In summary, we have used ultrafast time-resolved two-photon photoemission to observe the excited electron relaxation in GaAs(100). These are the first studies of semiconductor surfaces in which the temporal resolution has been sufficient to follow the non-equilibrium electron redistribution process evolving towards a Fermi–Dirac distribution. Electron lifetimes were obtained for states with energies ranging from the CBM to greater than 1.8 eV above the CBM, and show a pronounced dependence on the surface quality. Lifetimes ranging from less than 20 fs to greater than 400 fs were observed depending upon the energy of the intermediate state, and the quality of the material and surface. These results are consistent with the initial phase of thermalization being dominated by electron–electron scattering coupled with a strong dependence on the density of surface and defect states.

The most significant result of this work is that the surface quality and the bulk material quality dominate the relaxation rates of excited electrons near surfaces. These are the most important relaxation rates because electrons ultimately have to traverse surface interfaces in order to do anything useful in electrochemical, photochemical cells, or solid state devices. The TR-PES technique is ideal for fully characterizing electron dynamics at surfaces relevant to hot electron photochemistry because it provides information as a function of excited state energy with very high surface selectivity. The present work fully characterizes the relaxation dynamics of highly excited electrons with the appropriate spatial distribution along the surface normal and energy range to be correlated to the dynamics of hot electron photochemistry. This work, in combination with probes of

the charge transfer reaction dynamics, enables a determination of the relative importance of hot electron processes in the overall surface photochemistry.

Acknowledgements

This work was carried out under NSF Grant CHE-9120001 and DOE Grant No. DE-FG02-91ER14185. The authors would like to thank G. Wicks for preparing the MBE-grown surface QWs. The authors would also like to thank S.J. Diol for helpful discussions.

References

[1] J. Shah, Solid State Electron. 32 (1989) 1051. In addition, see Semiconductors probed by ultrafast laser spectroscopy, Vols. I and II, ed. R.R. Alfano (Academic Press, Orlando, 1984).
[2] T. Elsaesser, J. Shah, L. Rota and P. Lugli, Phys. Rev. Letters 66 (1991) 1757.
[3] Y. Rosenwaks, M.C. Hanna, D.H. Levi, D.M. Szmyd, R.K. Ahrenkiel and A.J. Nozik, Phys. Rev. B 48 (1993) 14675.
[4] W.S. Pelouch, R.J. Ellingson, P.E. Powers, C.L. Tang, D.M. Szmyd and A.J. Nozik, Phys. Rev. B 45 (1992) 1450.
[5] A. Leitenstorfer, A. Lohner, T. Elsaesser, S. Haas, F. Rossi, T. Kuhn, W. Klein, G. Boehm, G. Traenkle and G. Weimann, Phys. Rev. Letters 73 (1994) 1687.
[6] P.C. Becker, H.L. Fragnito, C.H. Brito Cruz, J. Shah, R.L. Fork, J.E. Cunningham, J.E. Henry and C.V. Shank, Appl. Phys. Letters 53 (1988) 2089.
[7] U. Hohenester, P. Supancic, P. Kocevar, X.Q. Zhou, W. Kütt and H. Kurz, Phys. Rev. B 47 (1993) 13233.
[8] A.J. Taylor, D.J. Erskine and C.L. Tang, J. Opt. Soc. Am. B 2 (1985) 663.
[9] M.J. Rosker, F.W. Wise and C.L. Tang, Appl. Phys. Letters 49 (1986) 1726.
[10] M. Ulman, D.W. Bailey, L.H. Acioli, F.G. Vallée, C.J. Stanton, E.P. Ippen and J.G. Fujimoto, Phys. Rev. B 47 (1993) 10267.
[11] U.D. Keil, D.R. Dykaar, R.F. Kopf and S.B. Darack, Appl. Phys. Letters 64 (1994) 3257.
[12] M. Koch, D. Weber, J. Feldman, E.O. Göbel, T. Meier, A. Schulze, P. Thomas, S. Schmitt-Rink and K. Ploog, Phys. Rev. B 47 (1993) 1532.
[13] P.C. Becker, H.L. Fragnito, C.H. Brito Cruz, R.L. Fork, J.E. Cunningham, J.E. Henry and C.V. Shank, Phys. Rev. Letters 61 (1988) 1647.
[14] K. Leo, M. Wegener, J. Shah, D.S. Chemla, E.O. Göbel, T.C. Damen, S. Schmitt-Rink and W. Schäfer, Phys. Rev. Letters 65 (1990) 1340.
[15] K. Leo, E.O. Göbel, T.C. Damen, J. Shah, S. Schmitt-Rink, W. Schäfer, J.F. Müller, K. Köhler and P. Ganser, Phys. Rev. B 44 (1991) 5726.
[16] A. Lohner, K. Rick, P. Leisching, A. Leitenstorfer, T. Elsaesser, T. Kuhn, F. Rossi and W. Stolz, Phys. Rev. Letters 71 (1993) 77.
[17] M.D. Webb, S.T. Cundiff and D.G. Steel, Phys. Rev. Letters 66 (1991) 934.
[18] J. Kuhl, E.J. Mayer, G. Smith, R. Eccleston, D. Bennhardt, P. Thomas, K. Bott and O. Heller, Semicond. Sci. Technol. 9 (1994) 429.
[19] D.S. Kim, J. Shah, T.C. Damen, W. Schäfer, F. Jahnke, S. Schmitt-Rink and K. Köhler, Phys. Rev. Letters 69 (1992) 2725.
[20] W.S. Fann, R. Storz, H.W.K. Tom and J. Bokor, Phys. Rev. B 46 (1992) 13592.
[21] R. Haight and M. Baeumler, Surface Sci. 287/288 (1993) 482.
[22] J.R. Goldman and J.A. Prybyla, Phys. Rev. Letters 72 (1994) 1364.
[23] C.A. Schmuttenmaer, M. Aeschlimann, H.E. Elsayed-Ali, R.J.D. Miller, D.A. Mantell, J. Cao and Y. Gao, Phys. Rev. B 50 (1994) 8957.
[24] R. Haight and J.A. Silberman, Phys. Rev. Letters 62 (1989) 815.
[25] J. Bokor, Science 246 (1989) 1130.
[26] E. Knoesel, T. Hertel, M. Wolf and G. Ertl, Chem. Phys. Letters 240 (1995) 409.
[27] D. Wang, J. Buontempo, Z.W. Li and R.J.D. Miller, Chem. Phys. Letters 232 (1995) 7.
[28] D.S. Boudreaux, F. Williams and A.J. Nozik, J. Appl. Phys. 51 (1980) 2159.
[29] R.L. Fork, O.E. Martinez and I.P. Gordon, Opt. Letters 9 (1984) 150.
[30] Gary Wicks at the Molecular Beam Epitaxial Laboratory, The Institute of Optics, University of Rochester, Rochester, NY 14627.
[31] F.J. Himpsel, Advan. Phys. 32 (1983) 1.
[32] J.R. Chelikowsky and M.L. Cohen, Phys. Rev. B 14 (1976) 556.
[33] C. Cameron Miller, C.A. Schmuttenmaer, J. Cao, D.A. Mantell, Y. Gao and R.J.D. Miller, in preparation.
[34] M.H. Hecht, Phys. Rev. B 41 (1990) 7918.
[35] A.S. Grove, Physics and technology of semiconductor devices (Wiley, New York, 1967); S.M. Sze, Physics of semiconductor devices (Wiley, New York, 1981).
[36] I.M. Vitomirov, A. Raisanen, A.C. Finnefrock, R.E. Viturro, L.J. Brillson, P.D. Kirchner, G.D. Perttit and J.M. Woodall, Phys. Rev. B 46 (1992) 13293.
[37] D.E. Aspnes and A.A. Studna, Phys. Rev. B 27 (1983) 985.
[38] G. Friedlander, Nuclear and radiochemistry (Wiley, New York, 1981).
[39] It should be noted that the high electronic temperature estimated for this data is significantly higher than our previous studies of metals. The differences lies in the density of electronic states which determines the temperature.
[40] X. Zhou and T.Y. Hsiang, J. Appl. Phys. 67 (1990) 7399; X.

Zhou, T.Y. Hsiang and R.J.D. Miller, J. Appl. Phys. 66 (1989) 3066.
[41] R.E. Viturro, J.M. Woodall, S.L. Wright, G.D. Pettit, J.L. Shaw, P.D. Kirchner and L.J. Brillson, J. Vacuum Sci. Technol. B 6 (1988) 1397.
[42] R.E. Viturro, J.L. Shaw, C. Mailhiot, L.J. Brillson, N. Tache, J. McKinley, G. Margaritondo, J.M. Woodall, P.D. Kirchner, G.D. Pettit and S.L. Wright, Appl. Phys. Letters 52 (1988) 2052.
[43] D. Pines and P. Nozières, The theory of quantum liquids (Benjamin, New York, 1966).
[44] J.J. Quinn, Phys. Rev. 126 (1962) 1453.
[45] J. Cao, D.A. Mantell, Y. Gao and R.J.D. Miller, to be submitted.